

Article

Coupled Vibration Analysis of Multi-Span Continuous Cable Structure Considering Frictional Slip

Zhongchu Tian^{1,2} and Binlin Xu^{1,*} 

¹ School of Civil Engineering, Changsha University of Science & Technology, Changsha 410114, China; tianzhongchu@163.com

² School of Civil Engineering, Fujian University of Technology, Fuzhou 350118, China

* Correspondence: xubinlin@stu.csust.edu.cn; Tel.: +86-186-9208-3845

Abstract: As important load-bearing structures, suspension cables have been widely used in suspension bridges, engineering ropeways, cable suspension systems and other special equipment. Their dynamic problems have always been a research hotspot. Especially for complex cable systems such as engineering ropeways and cable lifting equipment, there will be moving loads acting on multi-span continuous friction-slip cable structures, resulting in nonlinear coupled vibration. Therefore, few scholars have studied how to calculate the nonlinear coupling vibration effect between such moving loads and multi-span continuous cables considering friction slip. Therefore, this paper proposes the use of the combination of the direct stiffness method and the Newmark- β integration method to solve the nonlinear system of equations of motion, which can be derived from the coupled vibration response between the moving load and the main cable. The corresponding calculation program is prepared. Combined with the dynamic load test and simulation results of engineering cases, the correctness and reasonableness of the coupled vibration equations and the program can be verified through comparative analysis. The results show that the calculation results of the self-programmed program are in good agreement with the dynamic load test results, in which the maximum error of the vertical displacement in the span is -4.40% and 0.86% , and the error of the static calculation reaches -13.90% . The impact effect is more obvious when hoisting the weight out of the pulling cable, in which the impact coefficient of the main cable can be up to 2.0. The impact coefficient of the deviation of the cable tower is 4.0. During the traveling process of the moving load, the vertical downward deflection of the main cable at the action point is the largest, and the upward deflection is in the region of $0.2\sim 0.8L$ from the action point.

Keywords: frictional slip; nonlinear coupled vibration; Newmark- β ; dynamic load test; moving load



Citation: Tian, Z.; Xu, B. Coupled Vibration Analysis of Multi-Span Continuous Cable Structure Considering Frictional Slip. *Appl. Sci.* **2024**, *14*, 2215. <https://doi.org/10.3390/app14052215>

Academic Editor: Alexander N. Pisarchik

Received: 15 February 2024

Revised: 28 February 2024

Accepted: 5 March 2024

Published: 6 March 2024



Copyright: © 2024 by the authors. Licensee MDPI, Basel, Switzerland. This article is an open access article distributed under the terms and conditions of the Creative Commons Attribution (CC BY) license (<https://creativecommons.org/licenses/by/4.0/>).

1. Introduction

Suspension cables are widely used in suspension bridges, cable-stayed bridges, engineering ropeways, cable hoisting systems and other structures because of their strong tensile properties, large spans and ease of construction and fabrication. Suspension cables, as flexible materials, with long and elastic cables and low damping, have obvious nonlinear effects under the excitation of external loads. Especially for complex cable systems such as engineering ropeways and cable lifting equipment, there will be moving loads acting on multi-span continuous friction-slip cable structures, resulting in nonlinear coupled vibration. Therefore, few scholars have studied how to calculate the nonlinear coupling vibration effect between such moving loads and multi-span continuous cables considering friction slip. This paper takes a cable hoisting system, which is a special piece of equipment for bridges, as the background for carrying out research.

The cable hoisting system mainly consists of cable towers, anchorages, main cables, hoisting cables, pulling cables, fixed saddles, traveling cranes (Figure 1), spreaders, hoisting and traction winches, automation control systems and other major systems [1,2] (Figure 2).

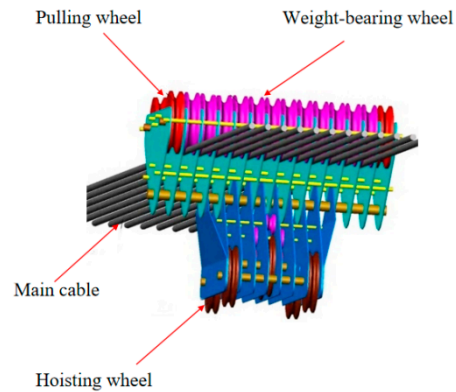


Figure 1. Traveling crane.

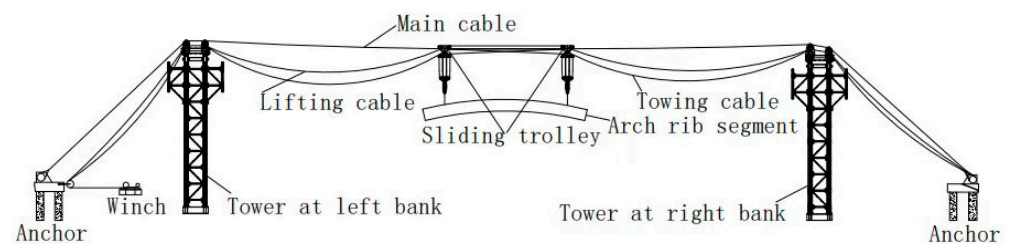


Figure 2. Cable hoisting system.

When the crane is traveling with a load, the main cable under its action will be forced to vibrate, resulting in a load greater than the static load under the action of deformation and internal force; this phenomenon is the “coupling vibration” effect. Since the main cable is pulley-supported at the top of the cable tower (as shown in Figure 3), the main cable will produce relative sliding at the saddle when the crane is traveling. However, the friction between the main cable and the saddle will lead to longitudinal deflection of the cable tower. So, the forced vibration of the main cable will be different from the single cable vibration.



Figure 3. Fixed saddle.

Flexible suspension cables are susceptible to complex coupled vibrations under moving load excitation. The coupled vibration response between the main cable and the moving load can be analyzed with reference to the theory of coupled vibration of a vehicle and bridge, but they are different. The differences are as follows: First, the bridge structure is rigid, with strong bending performance, while the cable structure is a flexible material with strong geometric nonlinearity. Second, the boundary conditions are different. When analyzing the coupled vibration of a vehicle and bridge, the bridge structure is generally constrained to the longitudinal displacement. For the coupled vibration of a moving load and cable, the two ends are in a relative slip. Therefore, in order to investigate the response

mechanism of coupled vibration, two major difficulties need to be solved. One is the problem of geometric nonlinearity and relative slip of the cable structure, and the other is the dynamic characteristics of the cable structure.

In order to model the sliding friction action of cable structures, many scholars have also proposed their own theories and insights. Chung et al. developed a three-dimensional cable element considering frictional slip based on the theory of catenaries, which provided research ideas for subsequent scholars, but only for two-node catenary cable elements, which are not adapted to multi-node continuous cable structures [3]. Kan et al. proposed a new multi-node sliding catenary cable element to solve the slipping problem that exists in the main cables of the cable hoisting system. But the element does not take into account the friction effect of the cables [4]. Nizar et al. proposed an accurate finite element method for continuous cable structures based on the suspension line theory and the Euler–Eytelwein equation with consideration of sliding friction, but they did not consider temperature effects [5,6]. Yang et al. proposed a finite element formulation for cable structures that takes into account the effects of temperature and sliding friction. The equation overcomes the limitations of existing methods that ignore or approximate friction, pulley size, temperature and geometric nonlinearities [7].

For the dynamic response of suspension cables under external load excitation, scholars have carried out a large number of experimental and theoretical studies. Irvine and Caughey put forward the linear theory of free vibration by conducting free vibration experiments on a single-curved suspension structure [8,9]. However, the suspension cables themselves have strong geometric nonlinearities, and the nonlinearities have a large influence on the vibration of the cables. So, the geometric nonlinearities of the suspension cables cannot be ignored in the research process. Luongo et al. started to extend the linear vibration study of the suspension cables to the geometric nonlinearities by utilizing the Galyokin method [10]. Subsequently, researchers used a variety of methods to study the free vibration, nonlinear periodic and semi-periodic vibration characteristics of suspension cables [11–14]. In this aspect of research, the first use of a multi-degree-of-freedom discrete model with a linear modal deviation function was Green's program applied to partial differential control equations and the use of multiple scaling methods to obtain the expected vibration response.

The above solution of nonlinear vibration equations for suspension structures is only applicable in the case of weak nonlinearity. In order to analyze the strong nonlinear vibration effects of suspension cable structures, researchers used vibration differential equations and finite elements combined with the direct integration method. Wu and Chen analyzed the vibration response of suspension cables due to dynamic loads by using the Newmark direct integration combined with the Newton–Raphson iteration method [15]. Larsen and Nielsen discretized the cable structure into a two-degree-of-freedom system and analyzed the vibration response of the structure under nonlinear excitation by the MCS method [16]. But this method is prone to convergence difficulties. In addition, the virtual force method [17,18] and the incremental superposition technique [19,20] have also been applied to the nonlinear vibration response analysis of suspension cables. Brennan and Kovacic obtained the vibration differential equations of a cable structure in the undamped case and solved the intrinsic frequency and characteristic equations of the cable structure by using transcendental equations [21]. Luo et al. analyzed the effect of nonlinear coupled vibration using a multiscale model order reduction strategy, which solved the problem of error and convergence difficulty brought by the finite method [22]. However, these studies all analyzed single cable structures for multi-span continuous complex cable systems. Han F et al. proposed using the dynamic stiffness method to calculate the vibration equations of a cable structure in the damped case and established the relationship between the damped frequency and the undamped frequency [23–26]. However, this method cannot calculate the slip state of a complex cable system at the support.

In summary, for a multi-span continuous complex cable system, to calculate the nonlinear coupled vibration response of the suspension structure under the consideration

of the friction–slip state, it is still necessary to discretize the cable structure by using the finite element method and then solve it by using the method of direct integration over the time step. This paper simulates the slip of the main cable at the top of a cable tower by drawing on the three-node slip cable element. The two–node catenary cable element simulates the nonlinearity of the main cable, coupled to form a subsystem model of the main cable structure, and is combined with the direct stiffness method to establish a system model of the moving load. By analyzing the force relationship between the moving load and the main cable, the coupled vibration dynamics of the moving load and the cable are deduced to control equations. Based on the Newmark– β direct integration method combined with the dynamic stiffness method, the nonlinear system of equations of motion is solved. The coupled vibration response between the moving load and the main cable can be obtained when the crane is traveling with a load. The corresponding calculation program is compiled. Combined with the dynamic load test and simulation results of engineering cases, the correctness and feasibility of the vibration equations and the program can be verified by comparing and analyzing the finite element calculation results, the dynamic load test values and the program calculation results.

2. Nonlinear Coupled Vibration Model

2.1. Moving Load Model

The main cable of the cable hoisting system can slide at the cable saddle at the top of the cable tower, and the crane only operates with a load in the mid–span. So, this paper only considers the coupling vibration between the crane and the main cable in the mid–span, in order to establish the dynamic control equations of the crane–cable coupling vibration. The computational model of the main cable under the action of the crane traveling with a load is shown in Figure 4. In the figure, points A and D are fixed, and the main cable can produce x –direction sliding at points B and C. The main cable can also slide in the x –direction. In order to further establish a model close to the actual cables, the hoisting cables between the crane and the hoisting section are considered as springs and damping devices, so as to establish the model as shown in the figure below. The moving load on the main cables consists of the two traveling crane masses m_1 and m_2 and the hoisting section m_3 . The mass moment of inertia I_3 is due to the fact that m_3 is connected between two axes at a certain distance, which generates the mass moment of inertia I_3 . The two cranes are connected to the hoisting arch section by the damper c_1 , spring k_1 , damper c_2 and spring k_2 . The distance between the two traveling cranes is a . It is assumed that the cranes do not separate from the main cables during the moving process. Let the modulus of elasticity of the main cable be E , the area be A , the damping coefficient be C and the mass per unit length of the cable be m .

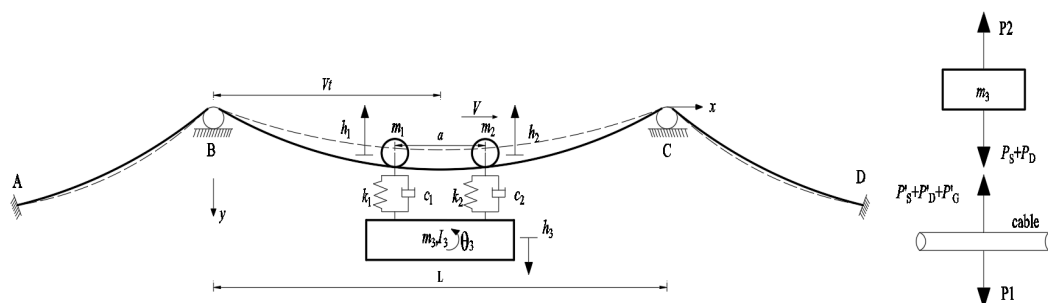


Figure 4. Calculation model of the main cable under the action of crane with a load movement.

Since the speed of the crane is very small when it is traveling with a load, it is assumed that the crane travels at a constant speed with a speed V and moves a distance $x = Vt$, and the main cable produces only a vertical dynamic deflection of u_b without bending deformation. The vertical dynamic displacement of the hoisting arch section m_3 is h_3 , the rotational displacement θ , and the vertical dynamic displacements of the two cranes

are h_1 and h_2 . Then, the force acting on the undersprung mass m_3 has the inertial force $P_2 = (m_3 + I_3)\ddot{u}_v$. The forces of m_1 and m_2 include inertial forces $P_1 = (m_1 + m_2)\ddot{u}_v$, elastic forces generated by hoisting cables $P_S = (k_1 + k_2)(u_v - u_b)|_{x=Vt}$, damping forces generated by hoisting cables $P_D = (c_1 + c_2)(\dot{u}_v - \dot{u}_b)|_{x=Vt}$. The equation of motion for m_3 can be obtained from the force balance of m_3 as [27]

$$[M_v]\{\ddot{u}_v\} + [C_v]\{\dot{u}_v\} + [K_v]\{u_v\} = 0 \tag{1}$$

where M_v is the mass matrix of the moving load model, C_v is the damping matrix of the moving load model and K_v is the stiffness matrix of the moving load model.

$$[M_v] = \begin{bmatrix} m_3 & 0 & 0 & 0 \\ 0 & I_3 & 0 & 0 \\ 0 & 0 & m_1 & 0 \\ 0 & 0 & 0 & m_2 \end{bmatrix}, [C_v] = \begin{bmatrix} c_1 + c_2 & (c_1 - c_2)\frac{a}{2} & -c_1 & -c_2 \\ (c_1 - c_2)\frac{a}{2} & (c_1 + c_2)(\frac{a}{2})^2 & -c_1\frac{a}{2} & c_2\frac{a}{2} \\ -c_1 & -c_1\frac{a}{2} & c_1 & 0 \\ -c_2 & c_2\frac{a}{2} & 0 & c_2 \end{bmatrix},$$

$$[K_v] = \begin{bmatrix} k_1 + k_2 & (k_1 - k_2)\frac{a}{2} & -k_1 & -k_2 \\ (k_1 - k_2)\frac{a}{2} & (k_1 + k_2)(\frac{a}{2})^2 & -k_1\frac{a}{2} & k_2\frac{a}{2} \\ -k_1 & -k_1\frac{a}{2} & k_1 & 0 \\ -k_2 & k_2\frac{a}{2} & 0 & k_2 \end{bmatrix}$$

2.2. Main Cable Subsystem Model

With the direct stiffness method, the main cable subsystem model of the cable hoisting system is established. According to what was assumed earlier, when the crane passes through the main cable with speed V , the main cable is subjected to the force of gravity $F_g = (m_1 + m_2 + m_3 + I_3)g$ and hoisting cable elastic force $P_S = k_v(u_v - u_b)|_{x=Vt}$. The damping force of the hoisting cables is $P_D = c_v(\dot{u}_v - \dot{u}_b)|_{x=Vt}$.

So, $F_b = \delta(x - Vt)[m_v g + k_v(u_v - u_b) + c_v(\dot{u}_v - \dot{u}_b)]$. The equation of motion of the main cable under a uniformly moving load can be expressed as

$$[M_b]\{\ddot{u}_b\} + [C_b]\{\dot{u}_b\} + [K_b]\{u_b\} = \{F_b\} \tag{2}$$

where M_b is the mass matrix of the main cable subsystem model, C_b is the damping matrix of the main cable subsystem model, K_b is the stiffness matrix of the main cable subsystem model, F_b is the external load vector.

In order to consider the nonlinearity and slip effects of the main cable of the cable hoisting system, the whole main cable is now discretized into two three-node catenary slip cable elements (i.e., span anchorage node, slip node at the top of the cable tower and node of the mid-span cable closest to the cable tower) and $m-2$ two-node catenary cable elements. The tangent stiffness matrices and damping matrices of the two types of elements are briefly described in the following subsections.

2.2.1. Two-Node Catenary Cable Element

Figure 5 shows a two-node planar catenary cable element; A and B are the two nodes of the element, and the curve equation of the element is [28]

$$\begin{cases} l = -\frac{F_1 s}{EA} - \frac{F_1}{q} \ln\left(\frac{T_A + F_2}{T_B - F_4}\right) \\ h = -\frac{F_2 s}{EA} + \frac{qs^2}{2EA} + \frac{T_B - T_A}{q} \end{cases} \tag{3}$$

where q , E , A and s are the load set, modulus of elasticity, area and unstressed length of the cable, respectively. $F_1 \sim F_4$ are the nodal component forces of the cable. $F_3 = -F_1$; $F_4 = qs - F_2$. T_A and T_B are the cable forces at nodes A and B , respectively.

$$\begin{cases} T_A = \sqrt{F_1^2 + F_2^2} \\ T_B = \sqrt{F_3^2 + F_4^2} \end{cases} \quad (4)$$

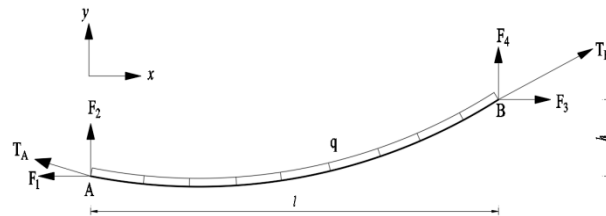


Figure 5. Two-node plane cable element.

Differentiating Equation (3) results in

$$\begin{pmatrix} dl \\ dh \end{pmatrix} = \begin{bmatrix} f_{11} & f_{12} \\ f_{21} & f_{22} \end{bmatrix} \begin{pmatrix} dF_1 \\ dF_2 \end{pmatrix} = F \begin{pmatrix} dF_1 \\ dF_2 \end{pmatrix} \quad (5)$$

where $f_{11} = -\left[\frac{s}{EA} + \frac{1}{q} \ln\left(\frac{T_A + F_2}{T_B - F_4}\right)\right] + \frac{F_1^2}{q} \left[\frac{1}{T_B(T_B - F_4)} - \frac{1}{T_A(T_A + F_2)}\right]$, $f_{12} = f_{21} = \frac{F_1}{q} \left(\frac{1}{T_B} - \frac{1}{T_A}\right)$, $f_{33} = -\frac{s}{EA} - \frac{1}{q} \left(\frac{F_4}{T_B} + \frac{F_2}{T_A}\right)$.

The stiffness matrix of a cable element can be solved by the inverse matrix of its flexibility matrix:

$$[K] = [F]^{-1} = \begin{bmatrix} f_{11} & f_{12} \\ f_{21} & f_{22} \end{bmatrix}^{-1} \quad (6)$$

The nodal force vectors of the elements can also be obtained as

$$\{F_{int}\} = \{F_1 \quad F_2 \quad F_3 \quad F_4\}^T \quad (7)$$

The tangent stiffness matrix of the element can be solved by Newton–Raphson iteration; the initial value of the iteration and the iteration procedure can be found in the literature [28].

The damping matrix of the element is

$$C = c \begin{bmatrix} 1 & 0 & -1 & 0 \\ 0 & 0 & 0 & 0 \\ -1 & 0 & 1 & 0 \\ 0 & 0 & 0 & 0 \end{bmatrix} = \begin{bmatrix} c_{11} & c_{12} \\ c_{21} & c_{22} \end{bmatrix} \quad (8)$$

where c is the viscous damping coefficient of the element in units of force \times time \times length.

2.2.2. Three–Node Sliding Cable Element

The main cables are often capable of sliding at the saddle at the top of the cable tower during the operation of the cable hoisting system under load. In the main cable design, the total stress-free length of the three-span continuous cable is usually given. The three-node sliding cable unit is shown in Figure 6, with I , O and J as the three nodes of the element, where point O is the sliding node. A pulley is usually designed to realize the sliding. The element is composed of the left IO cable section and the right OJ cable section. The element considers sliding friction.

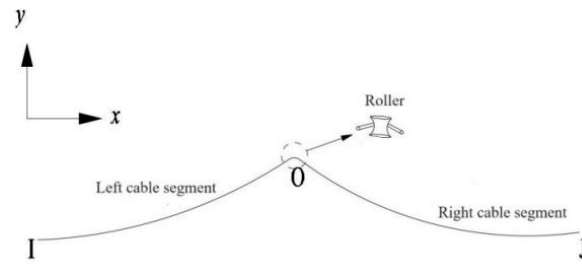


Figure 6. Three-node sliding cable element.

The three-node catenary cable element shown in Figure 6 is analyzed separately as shown in Figure 7, which is shown by the curve equations of the cable segments [7]:

$$\begin{cases} l_{x1} = -\frac{F_1 s_1}{EA} - \frac{F_1}{q} \ln\left(\frac{T_A + F_2}{T_B - F_4}\right) \\ l_{y1} = -\frac{F_2 s_1}{EA} + \frac{q s_1^2}{2EA} + \frac{T_B - T_A}{q} \end{cases}, \begin{cases} l_{x2} = -\frac{F'_1 s_2}{EA} - \frac{F'_1}{q} \ln\left(\frac{T'_A + F'_2}{T'_B - F'_4}\right) \\ l_{y2} = -\frac{F'_2 s_2}{EA} + \frac{q s_2^2}{2EA} + \frac{T'_B - T'_A}{q} \end{cases} \quad (9)$$

where s_1 and s_2 are the unstressed cable lengths of the IO and OJ sections, respectively. q is the load set of the cable. $f_3 = -F_1, F_4 = q s_1 - F_2; F'_3 = -F'_1, F'_4 = q s_2 - F'_2$.

$$\begin{cases} T_A = \sqrt{F_1^2 + F_2^2} \\ T_B = \sqrt{F_3^2 + F_4^2} \end{cases}, \begin{cases} T'_A = \sqrt{F'^2_1 + F'^2_2} \\ T'_B = \sqrt{F'^2_3 + F'^2_4} \end{cases} \quad (10)$$

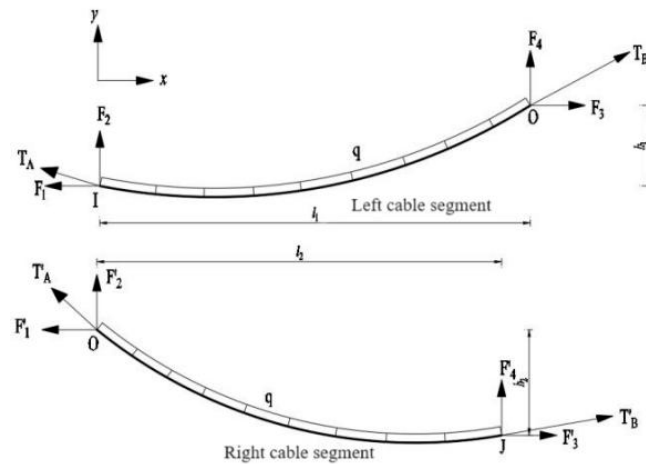


Figure 7. Force decomposition of three-node sliding cable element.

It follows from the constant length of unstressed cords on either side of node O that

$$s_1 + s_2 = s_0 \quad (11)$$

where s_0 is the unstressed cable length of the cable element, which is given as a known quantity during the division of the element.

The tension equilibrium of the two cable segments at the slip node O can be obtained by considering the dynamic friction:

$$T'_A = T_B e^{-\psi \mu \theta} \quad (12)$$

where θ is the angle between the cable end forces on both sides of the slip node.

$$\theta = \arccos\left(\frac{F_1 F'_1 + F_2 F'_2 + (F_3 - q_1 s_1) F'_3}{T_B T'_A}\right) \quad (13)$$

The direction function ψ is

$$\rho = \begin{cases} 1, & T_B > T'_A \\ 0, & T_B = T'_A \\ -1, & T_B < T'_A \end{cases} \tag{14}$$

From Equations (10)–(14), the basic set of equations for the sliding cable element can be formed:

$$\begin{cases} G_1 = x_I - x_O + l_{x1} \\ G_2 = y_I - y_O + l_{y1} \\ G_3 = x_O - x_J + l_{x2} \\ G_4 = y_O - y_J + l_{y2} \\ G_5 = s_1 + s_2 - s_0 \\ G_6 = T_B - T'_A \end{cases} \tag{15}$$

Here, $\mathbf{Z} = [F_1, F_2, F'_1, F'_2, s_1, s_2]^T$, $\mathbf{G} = [G_1, G_2, G_3, G_4, G_5, G_6]^T$.

Equation (15) can be solved by Newton–Raphson iteration, where the initial value of the iteration in $F_1 = \frac{q l_1}{2\lambda}$, $F_2 = \frac{q}{2}[s_1 - h_1 \coth \lambda]$, $F'_2 = \frac{q}{2}[s_2 - h_2 \coth \lambda]$, $F'_1 = \frac{q l_2}{2\lambda}$, $s_2 = s_0 - s_1$,

$$s_1 = \begin{cases} L_1 \zeta s_0 / (L_1 + L_2), & L_1 \geq L_2 \\ s_0 - L_2 \zeta s_0 / (L_1 + L_2), & L_1 < L_2 \end{cases} .$$

$$\text{Here, } \lambda_0 = \begin{cases} 0.2 & \text{if } s_i \leq L_i, \quad i = 1, 2 \\ \sqrt{3 \left(\frac{s_i^2 - h_i^2}{L_i} - 1 \right)} & \text{if } s_i > L_i, \quad i = 1, 2 \end{cases} .$$

L_1 and L_2 are the chord lengths of the cable segments IO and OJ , respectively.

$$\zeta = \begin{cases} 0.1\gamma^{-0.5} + 0.9, & 1/9 \leq \gamma \leq 1 \\ 1.2, & 0 < \gamma < 1/9 \end{cases} , \text{ for } L_1 \geq L_2, \gamma = L_1/L_2 \text{ and vice versa.}$$

$$\begin{cases} \mathbf{Z}_{n+1} = \mathbf{Z}_n + \Delta \mathbf{Z}_n \\ \Delta \mathbf{Z}_n = -(\mathbf{A}_n)^{-1} \mathbf{G}_n \end{cases} \tag{16}$$

where $\mathbf{A} = \frac{\partial \mathbf{G}}{\partial \mathbf{Z}}$ and n is the number of iterations.

$$\mathbf{A} = \begin{bmatrix} -\left[\frac{s_1}{EA} + \frac{1}{q} \ln \left(\frac{T_A + F_2}{T_B - F_4} \right) \right] & \frac{F_1}{q} \left(\frac{1}{T_B} - \frac{1}{T_A} \right) & 0 & 0 & -F_1 \left(\frac{1}{EA} + \frac{1}{TB} \right) & 0 \\ \frac{F_1}{q} \left(\frac{1}{TB} - \frac{1}{TA} \right) & -\left[\frac{s_1}{EA} + \frac{1}{q} \ln \left(\frac{F_4}{TB} + \frac{F_2}{TA} \right) \right] & 0 & 0 & F_4 \left(\frac{1}{EA} + \frac{1}{TB} \right) & 0 \\ 0 & 0 & -\left[\frac{s_2}{EA} + \frac{1}{q} \ln \left(\frac{T'_A + F'_2}{T'_B - F'_4} \right) \right] & \frac{F'_1}{q} \left(\frac{1}{T'_B} - \frac{1}{T'_A} \right) & 0 & -F'_1 \left(\frac{1}{EA} + \frac{1}{T'_B} \right) \\ 0 & 0 & \frac{F'_1}{q} \left(\frac{1}{T'_B} - \frac{1}{T'_A} \right) & -\left[\frac{s_2}{EA} + \frac{1}{q} \ln \left(\frac{F'_4}{T'_B} + \frac{F'_2}{T'_A} \right) \right] & 0 & F'_4 \left(\frac{1}{EA} + \frac{1}{T'_B} \right) \\ 0 & 0 & 0 & 0 & 1 & 1 \\ F_1/T_B & -F_4/T_B & -F'_1/T'_A & -F'_2/T'_A & qF_4/T_B & 0 \end{bmatrix}$$

The node coordinates of the element are $\mathbf{x} = \{x_1, y_1, x_2, y_2, x_3, y_3\}^T$, $\mathbf{F} = \{F_1, F_2, F_3 + F'_1, F_4 + F'_2, F_3, F'_4\}^T$.

Therefore, the tangent stiffness matrix \mathbf{k} of the three–node sliding catenary cable element is expressed as

$$\mathbf{k} = -\frac{\partial \mathbf{F}_i}{\partial \mathbf{X}_j} = -\frac{\partial \mathbf{F}_i}{\partial \mathbf{Z}_m} \frac{\partial \mathbf{Z}_m}{\partial \mathbf{G}_n} \frac{\partial \mathbf{G}_n}{\partial \mathbf{X}_j} = -\mathbf{B} \mathbf{A}^{-1} \mathbf{D} \tag{17}$$

$$\text{where } \mathbf{B} = \begin{bmatrix} 1 & 0 & 0 & 0 & 0 & 0 \\ 0 & 1 & 0 & 0 & 0 & 0 \\ -1 & 0 & 1 & 0 & 0 & 0 \\ 0 & -1 & 0 & 1 & q & 0 \\ 0 & 0 & -1 & 0 & 0 & 0 \\ 0 & 0 & 0 & -1 & 0 & q \end{bmatrix}, \mathbf{D} = \begin{bmatrix} 1 & 0 & 0 & 0 & 0 & 0 \\ 0 & 1 & 0 & 0 & 0 & 0 \\ -1 & 0 & 1 & 0 & 0 & 0 \\ 0 & -1 & 0 & 1 & 0 & 0 \\ 0 & 0 & -1 & 0 & 0 & 0 \\ 0 & 0 & 0 & -1 & 0 & 0 \end{bmatrix},$$

$$\mathbf{k} = \begin{bmatrix} \mathbf{k}_{11} & \mathbf{k}_{12} & \mathbf{0}_{2 \times 2} \\ \mathbf{k}_{21} & \mathbf{k}_{22} & \mathbf{0}_{2 \times 2} \\ \mathbf{k}_{31} & \mathbf{k}_{32} & \mathbf{0}_{2 \times 2} \end{bmatrix} .$$

The tangent stiffness matrix of the above three-node catenary cable element can be solved by iteratively solving Equation (17). The nodal force vector $\{F\}$ can be solved by iteratively solving Equation (16), so the displacement increment $\{\Delta x\}$ of the element can be solved according to the finite element balance equation.

The damping matrix of the three-node catenary cable element can be expressed as

$$C = \begin{bmatrix} -c_{s1} & c_{s1} & \mathbf{0}_{2 \times 2} \\ c_{s1} & -c_{s1} - c_{s2} & c_{s2} \\ \mathbf{0}_{2 \times 2} & c_{s2} & -c_{s2} \end{bmatrix} \tag{18}$$

2.3. Establishment of Coupled Vibration Equations

Coupling the equations of motion of the crane and the main cables together yields

$$\begin{bmatrix} M_v & 0 \\ 0 & M_b \end{bmatrix} \cdot \begin{Bmatrix} \ddot{u}_v \\ \ddot{u}_b \end{Bmatrix} + \begin{bmatrix} C_v & C_{vb} \\ C_{bv} & C_b \end{bmatrix} \cdot \begin{Bmatrix} \dot{u}_v \\ \dot{u}_b \end{Bmatrix} + \begin{bmatrix} K_v & K_{vb} \\ K_{bv} & K_b \end{bmatrix} \cdot \begin{Bmatrix} u_v \\ u_b \end{Bmatrix} = \begin{Bmatrix} 0 \\ -F_g \end{Bmatrix} \tag{19}$$

where $\begin{bmatrix} M_v & 0 \\ 0 & M_b \end{bmatrix} = \begin{bmatrix} m_v & 0 & 0 & \cdots & 0 & 0 \\ 0 & m & 0 & \cdots & 0 & 0 \\ 0 & 0 & m & \cdots & 0 & 0 \\ \vdots & \vdots & \vdots & \ddots & \vdots & \vdots \\ 0 & 0 & 0 & \cdots & m & 0 \\ 0 & 0 & 0 & \cdots & 0 & m \end{bmatrix},$

$$\begin{bmatrix} C_v & C_{vb} \\ C_{bv} & C_b \end{bmatrix} = \begin{bmatrix} c_v & 0 & \cdots & -c_v & \cdots & 0 \\ 0 & c_{1,1} & \cdots & c_{1,i} & \cdots & c_{1,n} \\ \vdots & \vdots & \ddots & \vdots & \ddots & \vdots \\ -c_v & c_{i,1} & \cdots & c_{i,i} & \cdots & c_{i,n} \\ \vdots & \vdots & \ddots & \vdots & \ddots & \vdots \\ 0 & c_{n,1} & \cdots & c_{n,i} & \cdots & c_{n,n} \end{bmatrix},$$

$$\begin{bmatrix} K_v & K_{vb} \\ K_{bv} & K_b \end{bmatrix} = \begin{bmatrix} k_v & 0 & \cdots & -k_v & \cdots & 0 \\ 0 & k_{1,1} & \cdots & k_{1,i} & \cdots & k_{1,n} \\ \vdots & \vdots & \ddots & \vdots & \ddots & \vdots \\ -k_v & k_{i,1} & \cdots & k_{i,i} & \cdots & k_{i,n} \\ \vdots & \vdots & \ddots & \vdots & \ddots & \vdots \\ 0 & k_{n,1} & \cdots & k_{n,i} & \cdots & k_{n,n} \end{bmatrix}.$$

$\begin{bmatrix} K_v & K_{vb} \\ K_{bv} & K_b \end{bmatrix}$ are explained in Figure 8.

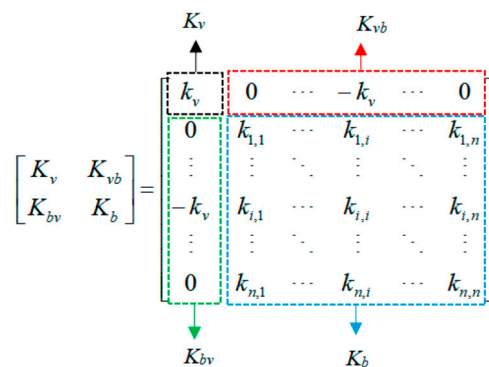


Figure 8. Decomposition diagram of the total stiffness matrix.

The basic steps for solving the forced vibration response of a multi-degree-of-freedom system are firstly, to determine the intrinsic properties of the system, then to establish the

decoupled modal equations of motion of the system and then to solve the equations according to the single-degree-of-freedom theory. If the system is subjected to a general excitation, the forced vibration response is attributed to the calculation of Duhamel convolution integrals, which not only is a cumbersome and lengthy process, but also often fails to find an analytical solution for the Duhamel integrals. Therefore, for this type of system of equations, the numerical method of stepwise integration can be used to solve the system [29].

3. Algorithms for Solving Nonlinear Systems of Time–Varying Equations

In a cable system with a single hoisting span of twin towers, the crane with a load only operates in the middle hoisting span. So, only the nonlinear coupled vibration response between the mid-span cables and the crane is analyzed. It is assumed that the main cables are able to slide in the position of the cable tower. Based on the Newmark- β direct integration method combined with the dynamic stiffness method, the nonlinear system of equations of motion is solved. The solution method and steps, for which the flow chart of crane–cable coupled vibration refinement analysis is shown in Figure 9, are as follows:

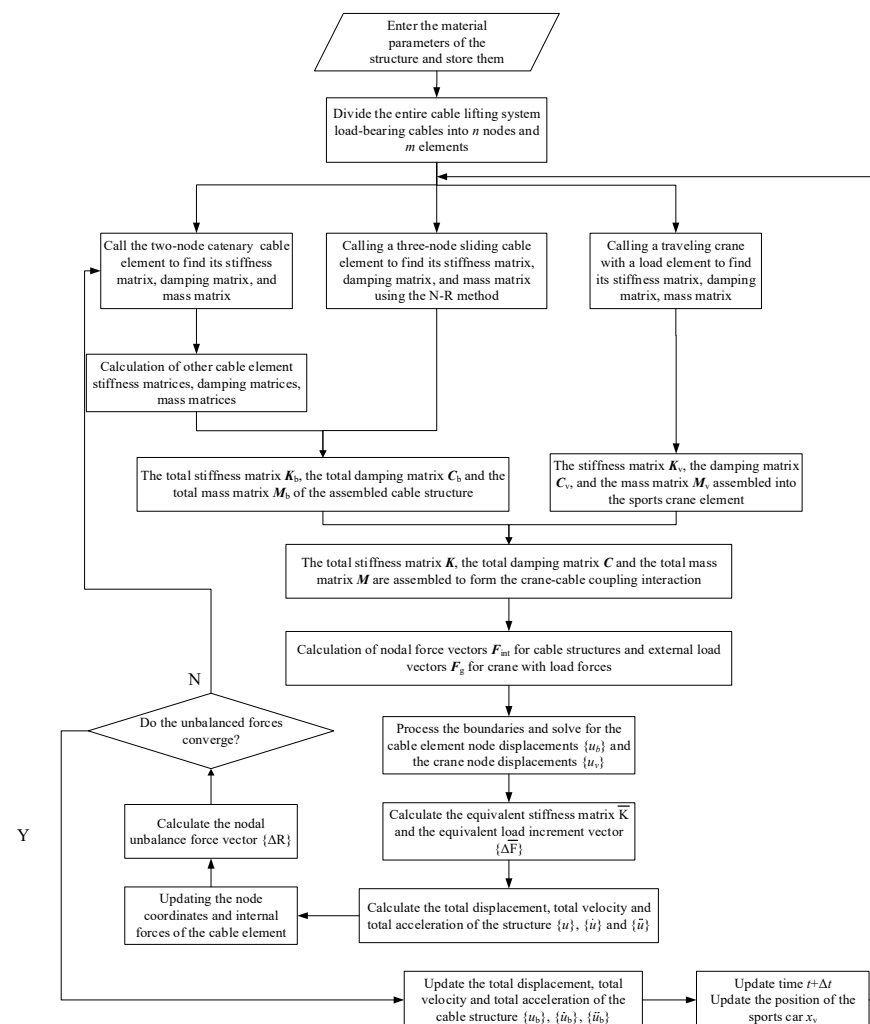


Figure 9. Flow chart of refined analysis of crane–cable coupling vibration.

- Firstly, select the Newmark parameters: β and γ . It is important to select the two parameters correctly, and the analysis shows that when $\gamma \geq 1/2$ and $\beta \geq \gamma/2$ are taken, the Newmark- β method is not able to be conditionally stabilized. Usually, $\gamma = 1/2$ is selected, and then β is adjusted to achieve the purpose of different corrections to

the acceleration. When $\gamma = 1/2$ and $\beta = \gamma/2$, it is linear acceleration method; when $\gamma = 1/2$ and $\beta = 1/6$, it is average acceleration method.

- (2) Time discretization: The studied motion time n is divided into equal parts with time step Δt ; the discrete points are $0, 1, 2, \dots, n - 1, n$. The time corresponding to the discrete points is $t_j = j\Delta t$ ($j = 0, 1, 2, \dots, n - 1, n$), with a start time $t_0 = 0$ and a termination time $t_m = n\Delta t$.
- (3) Each material parameter of the cable structure and the crane model (including the unstressed cable length s_0 of the cables) is entered and stored.
- (4) The whole cable sling is divided into n nodes and m elements, in which the mid-span cable is divided into $m - 2$ two-node catenary cable elements. The anchorage point of the side span, the top node of the cable tower and the node of the mid-span cable closest to the cable tower are divided into three-node catenary cable elements, with a total of two for the left and right side spans.
- (5) Call the model cell of the crane with a load and calculate its mass matrix M_v , stiffness matrix K_v and damping matrix C_v .
- (6) Call the two-node catenary cable element and the three-node catenary cable element and calculate their mass matrix, stiffness matrix and damping matrix, and then assemble them into the total mass matrix M_b , total stiffness matrix K_b and damping matrix C_b of the cable structure.
- (7) The main cable model is coupled and assembled with the crane model to form the total mass matrix M , the total stiffness matrix K and the damping matrix C .
- (8) Calculate the total nodal force vector F_{int} and the total external load vector (weight carried by the crane) F_g for the cable structure.
- (9) Process the boundary conditions to solve for the nodal displacements $\{u_b\}$ of the cable structure and the displacements $\{u_v\}$ of the crane model, and compose the total displacement vector $\{x\}$.
- (10) Calculate the initial motion parameters for the time step obtained from the previous time step: $\{x\}_j, \{\dot{x}\}_j, \{\ddot{x}\}_j$. When $j = 0$, the time step is obtained from the initial conditions: $\{x\}_0, \{\dot{x}\}_0, \{\ddot{x}\}_0 = [m]^{-1}[\{f\}_0 - [c]\{\dot{x}\}_0 - [k]\{x\}_0]$.
- (11) Calculate the time step termination motion parameters: ① Calculate the equivalent stiffness matrix and the equivalent load increment vector using Equation (20):

$$\begin{aligned} [\bar{K}] &= [K] + \frac{\gamma}{\beta\Delta t}[C] + \frac{1}{\beta\Delta t^2}[M] \\ \{\Delta\bar{F}\}_j &= [M]\left(\frac{1}{\beta\Delta t}\{\dot{x}\}_j + \frac{1}{2\beta}\{\ddot{x}\}_j\right) + [C]\left(\frac{\gamma}{\beta}\{\dot{x}\}_j + \left(\frac{\gamma}{2\beta} - 1\right)\Delta t\{\ddot{x}\}_j\right) + \{\Delta f\}_j \end{aligned} \quad (20)$$

- ② Calculate the displacement increment vector from Equation (21):

$$[\bar{K}]\{\Delta x(t)\} = \{\Delta\bar{F}(t)\} \quad (21)$$

- ③ Calculate the displacement increment vector $\{\Delta\dot{x}\}_j$ from Equation (22):

$$\{\Delta\dot{x}\}_j = \frac{\gamma}{\beta\Delta t}\{\Delta x\}_j - \frac{\gamma}{\beta}\{\dot{x}\}_j - \left(\frac{\gamma}{2\beta} - 1\right)\Delta t\{\ddot{x}\}_j \quad (22)$$

- ④ Calculate the displacement and velocity at the end of the current time step: $\{x\}_{j+1} = \{x\}_j + \{\Delta x\}_j, \{\dot{x}\}_{j+1} = \{\dot{x}\}_j + \{\Delta\dot{x}\}_j$.

- ⑤ Calculate the acceleration at the end of the current time step using Equation (23):

$$[M]\{\ddot{x}\}_{j+1} + [C]\{\dot{x}\}_{j+1} + [K]\{x\}_{j+1} = \{f\}_{j+1} \quad (23)$$

- (12) Update the nodal coordinates and internal forces of the cable element and calculate the nodal unbalanced force vector $\{\Delta R\}$.
- (13) Determine whether the unbalanced forces converge or not, i.e., whether $\frac{\|\Delta R\|}{\|F_g\|} \leq TOLER$. If 'Yes', update the displacement, velocity and acceleration of the cable

structure $\{u_b\}$, $\{\dot{u}_b\}$, $\{\ddot{u}_b\}$. If 'No', repeat steps (6) to (12) above until the unbalanced force converges.

- (14) Update time $t = t + \Delta t$ and update the overhead crane position Vt .
- (15) Repeat steps (5) through (14) above until all time steps have been calculated.

4. Engineering Examples

A double-tower, three-span cable hoisting system is taken as an engineering example, as shown in Figure 10. There is a fixed pulley on the top of each of the two towers, and the pulley can slide on the main cable during construction with considering sliding friction. The coordinates of the nodes are I(0, 43.038), J(96.1, 0), KL(96.1, 95.6), K(589.05, 3), KR(589.05, 95.6), L(712.2, 29.516). The main cable adopts nine $\phi 62$ steel cables with a tensile strength of 1870 MPa, an area of 0.016272 m², a weight per unit length of 1.497 kN/m and a modulus of elasticity of 110 GPa. The cable tower is made of Q345b steel, with a modulus of elasticity of 206 GPa. The designed maximum hoisting weight is 150 tons, and the crane weighs 8 tons. The original length of the middle-span cable is 494.8918 m, and the horizontal force is 2105.3 kN. The original length of the left-span cable is 109.4220 m. The original length of the right-span cable is 139.6430 m. According to the wire cable manufacturer's test, the damping coefficient of the wire cable is 0.3. The design speed of the traveling crane with a load is 0.16 m/s. The friction coefficient μ of the cable at the saddle is 0.3.

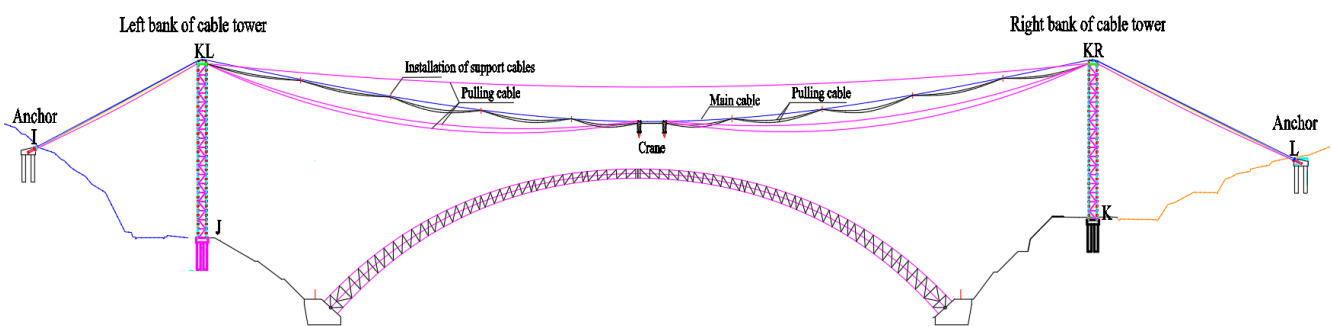


Figure 10. The double-tower, three-span cable hoisting system.

4.1. Dynamic Load Test for Cable Suspension

Test process:

- (1) First, consider the crane under the weight of 150 tons (100% of the rated hoisting weight).
- (2) Hoist the weight off the ground 10~20 cm and suspend it statically for 30 min. Consider all kinds of structures for visual inspection, the observation of all kinds of cable system connection statuses, etc. If there is no anomaly, you can carry out the next test.
- (3) Continue to lift the weight from the ground 3~5 m, for up and down movement. Detect the braking performance of the hoisting winch and hoisting speed.
- (4) Continue to lift the weight 2~3 m, for horizontal back-and-forth traction movement. With a traction range of 10~20 m, test the traction capacity and braking performance of traction winches and the traction speed of the crane.
- (5) Pull the weight to the L/2 span position and stop; measure the verticality at the main cable hoisting point, tower top offset, anchor displacement, cable force, etc.

4.1.1. Main Cable Sag Monitoring

The steel wire cable presents a catenary shape under the action of heavy loads, and the total station is used to measure and collect the sag of the main cable under various test load conditions. The total station is set up in prism-free test mode for prism-free measurement. The total station for plumbness monitoring is placed in the mid-span position of the existing highway bridge, which is the closest to the span of the main cable and convenient for measurement. With a single set of systems on both sides of the main

cable as the measurement of the reference cable, the main cable plumbing arrangement of the measurement point layout is shown in Figure 11.

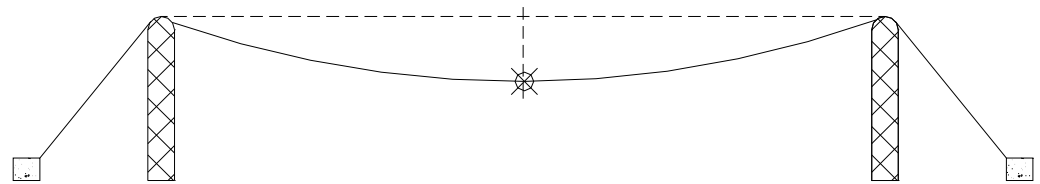


Figure 11. Layout of the main cable verticality measurement points.

4.1.2. Cable Force Monitoring

The main cable force is measured by the dynamic measurement method, and the monitoring instrument is the clueless force dynamic measurement module (JMCZ-2098AD/WD, Kingmach Measurement & Monitoring Technology Co., Ltd., Changsha, China), which is used to monitor the real-time cable force of the main cable under various loading conditions. The main cable force measurement points are arranged as shown in Figure 12.

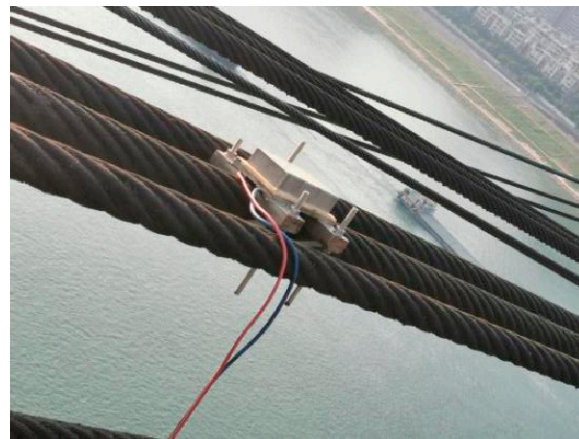


Figure 12. Layout of the cable force measurement points.

4.2. Finite Element Modeling

In order to verify the correctness of the coupled crane-cable vibration equation, a finite element model is established by ANSYS (Canonsburg, PA, USA) for the double-tower, three-span cable hoisting system (shown in Figure 13). The main cable is modeled by the link10 cable element; the cable tower is modeled by the Beam188 element. The top of the cable tower is modeled only by using the vertically pressurized spring element COMBIN14 to connect the main cable node with the cable tower; the crane and the heavy loads to be transported are modeled by the 2D mass element MASS21 without a rotational degree of freedom. The hoisting cable is modeled by the spring damping element COMBIN14. The movement of the mass spring is realized by means of the displacement coupling method, and the contact between the crane and the main cable is realized by means of a point-line contact element for the contact between the moving part and the cable.

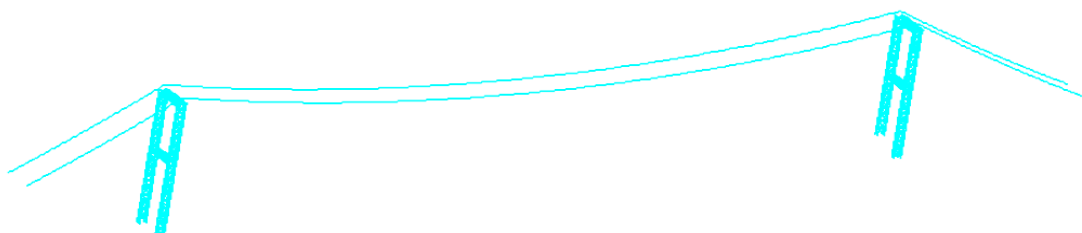


Figure 13. Finite element model.

The boundary conditions are as follows: the bottom of the cable tower is cemented, the main cables are cemented at the side spans, and the main cables are simulated with springs that are only vertically pressurized between the main cables and the cable tower. The speed of the moving load is 0.16 m/s, so the whole section of the main cable is encrypted, and the length of a single main cable element is 0.08 m. In order to simulate the slip state of the main cable at the support point, the cable element at the support point is also encrypted. In order to prevent the distortion of the cable tower members from stress concentration at the connection point, encryption treatment is also carried out. The whole cable hoisting system is discretized into 245,146 elements and 563,463 nodes.

4.3. Analysis of Results

In order to verify the correctness of the obtained coupled crane–cable vibration equations, the time–varying response of the whole process of the crane traveling with the load on the main cable at the mid–span is selected for analysis in this section. The total time spent by the crane from the left bank to the right bank under the design speed is 3080.94 s. In order to react to the vibration response when the lifted beam section is detached from the crane, a total time of 3600 s is taken for the analysis in this section, and the time step is taken to be 0.001 s. The dynamic load test value is based on the data measured when the crane is traveling to the L/4, 3L/8, 2/L, 3L/4 positions of the mid–span cable with a load.

4.3.1. Comparative Validation of Test Results

In order to analyze the coupled vibration response of a multi–span continuous cable structure under moving load, the mid–span vertical displacement and cable force of the main cable are selected as parameters for comparison in this section. Since the main cable is supported by pulleys at the top of the cable tower, when the crane is traveling, the main cable will produce relative friction slip at the saddle, and under the action of friction and unbalanced force at both ends of the saddle, the cable tower will be deformed. Therefore, in this section, the deflection of the cable tower is again selected as a parameter for comparative analysis. The data obtained by calculating each datum from the moment when the crane travels to the middle of the span are taken to be analyzed for the error, as shown in Table 1 and Figure 14.

Table 1. Comparison of errors of calculation methods.

Number	Calculation Parameters	Finite Element Calculated Values		Programmed Values		Static Values		Dynamic Load Test Values
		Values	Errors	Values	Errors	Values	Errors	
1	Vertical displacement/m	−9.631	−4.40% *	−10.161	0.86% *	−8.674	−13.90% *	−10.074
2	Mid–span forces/kN	4968.64	−2.77% *	5218.57	2.12% *	4646.25	−9.08% *	5110.12
3	Left–bank cable tower deviation/m	0.029	−4.29% *	0.0311	2.64% *	0.027	−10.89% *	0.0303
4	Right–bank cable tower deviation/m	−0.0386	−3.02% *	−0.0412	3.52% *	−0.0369	−7.29% *	−0.0398

* Error = (calculated value − dynamic load test value)/dynamic load test value.

From Figure 14 and Table 1, it can be seen that the simulation results and the program calculation results have the same trend. The calculation results of the self–programming program are more similar to the measured value, and the finite element calculation value results are large. Taking the maximum vertical displacement in the span as an example, the simulation calculation result is −9.631 m, and the measured value is −10.074 m. The program calculation result is −10.161 m, and the static calculation result is −8.674 m, and it can be seen that the simulation result and the program calculation result errors are −4.40% and 0.86%, while the static calculation result error reaches −13.90%, which causes this phenomenon. The reason for this phenomenon is that the coupled vibration caused by the non–uniform excitation of the main cable by the crane increases the vertical deflection, which also proves the correctness and feasibility of the deduced coupled vibration equations and the program calculation.

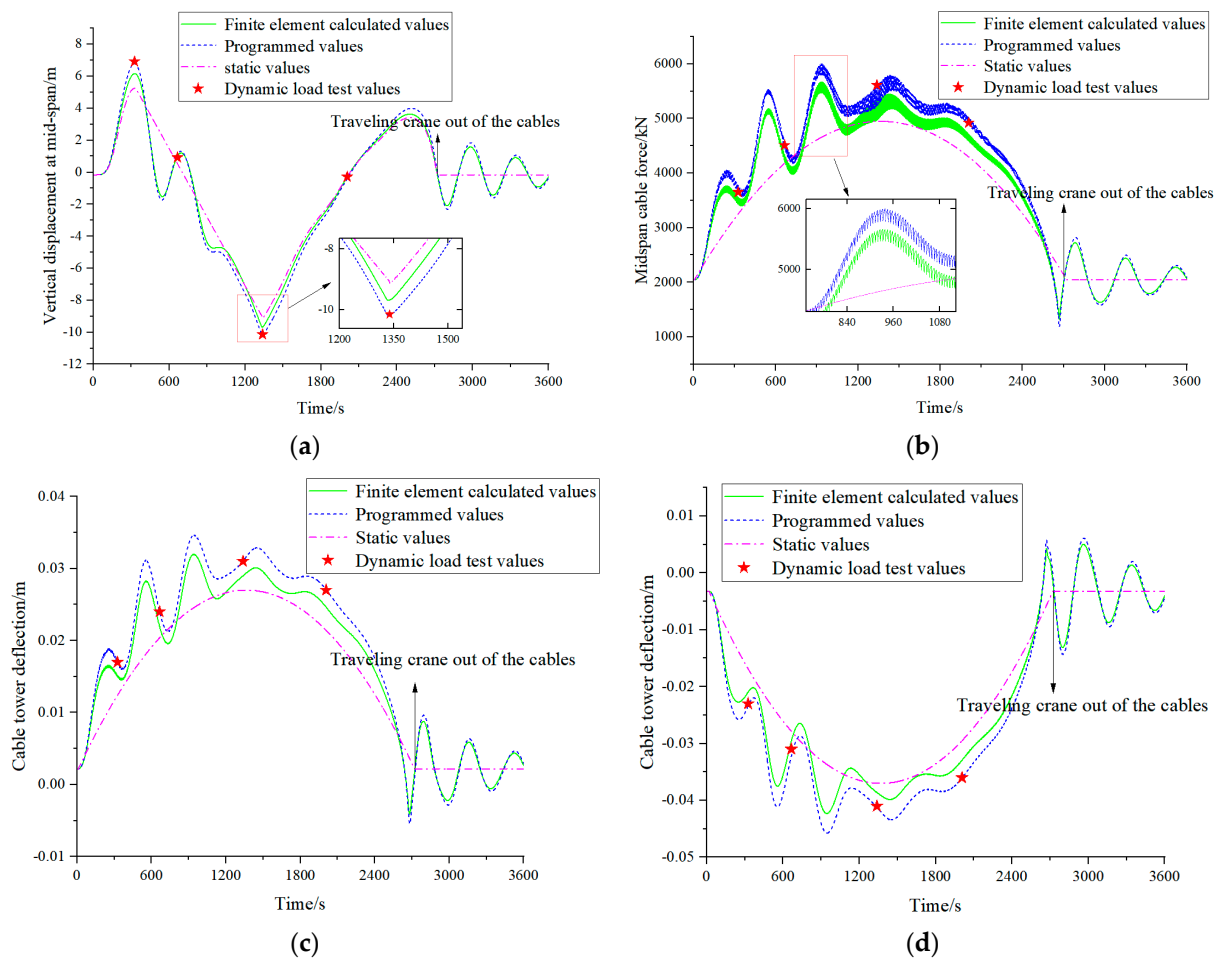


Figure 14. Comparison of results under the action of crane–cable coupled vibration at the design speed: (a) time course diagram of the vertical displacement in the span, (b) time course diagram of the cable force in the span, (c) time course diagram of the deflection of the left-bank cable tower, (d) time course diagram of the deflection of the right-bank cable tower.

4.3.2. Analysis of Impact Effect after Hoisting Weight Detachment

In order to investigate the impact effect generated by the cable hoist loading system when hoisting heavy loads out of the lifting cable, this section takes the hoisting of heavy loads from the left bank to the mid-span stage of detachment for analysis and obtains the mid-span displacement of the main cable, as shown in Figure 15.

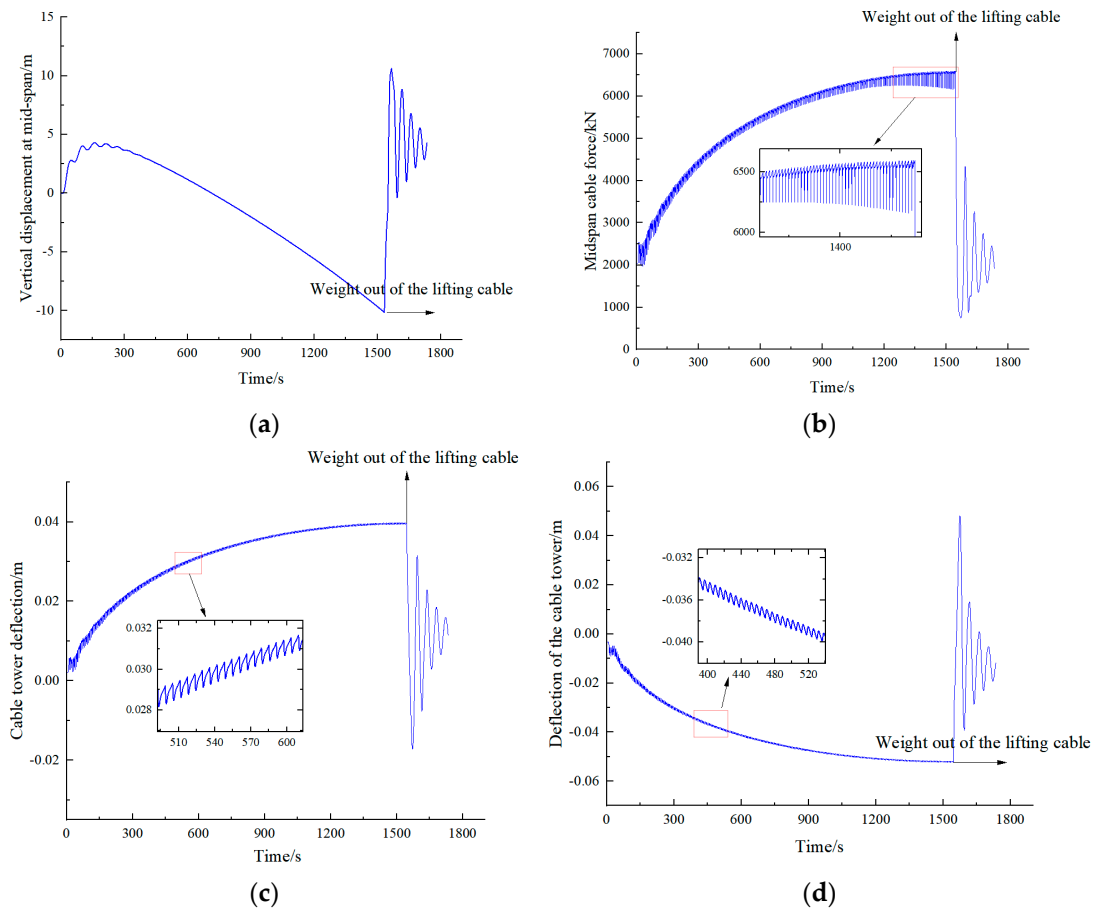


Figure 15. Diagram of the result of arch segments out of the lifting cable: (a) time course diagram of the vertical displacement in the span, (b) time course diagram of the cable force in the span, (c) time course diagram of the deviation of the left-bank cable tower, (d) time course diagram of the deviation of the right-bank cable tower.

As can be seen from Figure 15, the moment of hoisting the weight detached from the impact effect is very obvious. In order to describe the dynamic effect produced at the moment when the weight is detached from the pulling cable, this paper expresses it by calculating the impact coefficient μ . The ratio of the deflection or force added to the suspension structure at the moment the weight breaks away from the pulling cable to the deflection or force generated when the load is at rest is called the impact coefficient. The vertical maximum dynamic deflection generated in the span is up to 13.6 m, while the vertical static deflection generated only no-load action is only 4.78 m, with an impact coefficient of up to 2.0. The mid-span cable force generated by the maximum dynamic cable force is up to 4123 kN, and the no-load action generated by the static cable force is 1912 kN. The impact coefficient is 2.16. The left-bank cable tower maximum dynamic deflection is 0.031 m, and the no-load action generates a static deflection of 0.011 m. The impact coefficient is 2.82, and that on the left-bank cable tower is 2.16. The right-bank cable tower maximum dynamic deflection is 0.031 m, and no-load action produces a static deflection of 0.011 m; the impact coefficient of the left-bank cable tower is 2.82. The right-bank cable tower maximum dynamic deflection is 0.048 m, and no-load action produces a static deflection of 0.012 m; the impact coefficient of the left-bank cable tower is 4.00.

4.3.3. Vertical Displacement Analysis of Three-Span Continuous Main Cable

In order to explore the vertical displacement response of each span of the mid-span main cables under the non-uniform excitation of the crane, the displacement-time-span three-dimensional surface relationship is established in this section as shown in Figure 16.

From Figure 16, it can be seen that (1) during the traveling process of the crane with a load from the left bank to the right bank, the vertical downward deflection of the main cable at each moment of the crane's action point is the largest. But the other parts of the crane will show an upward deflection area, which mainly concentrates in the interval from the action point of $0.2\sim 0.8L$. The closer the point of action is to the center of the span, the smaller the upward deflection region will be. (2) When the crane is located in the middle of the span, the side-span cables are all in the upward deflection state and concentrate in the region of $0.2\sim 0.8L$. The side-span cables are the first ones that vibrate downward and reach the peak when the crane is driving away from the middle of the span main cables.

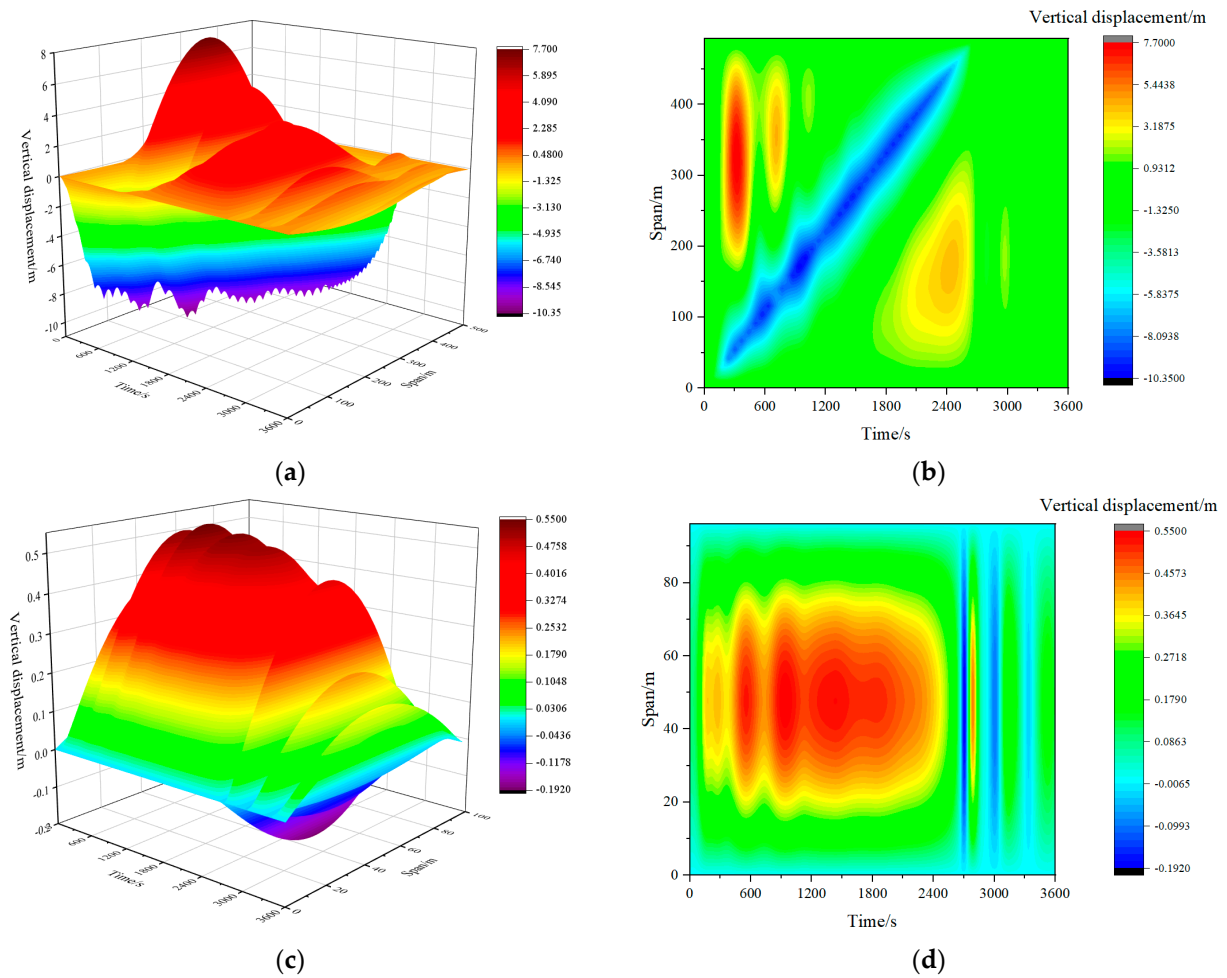


Figure 16. Cont.

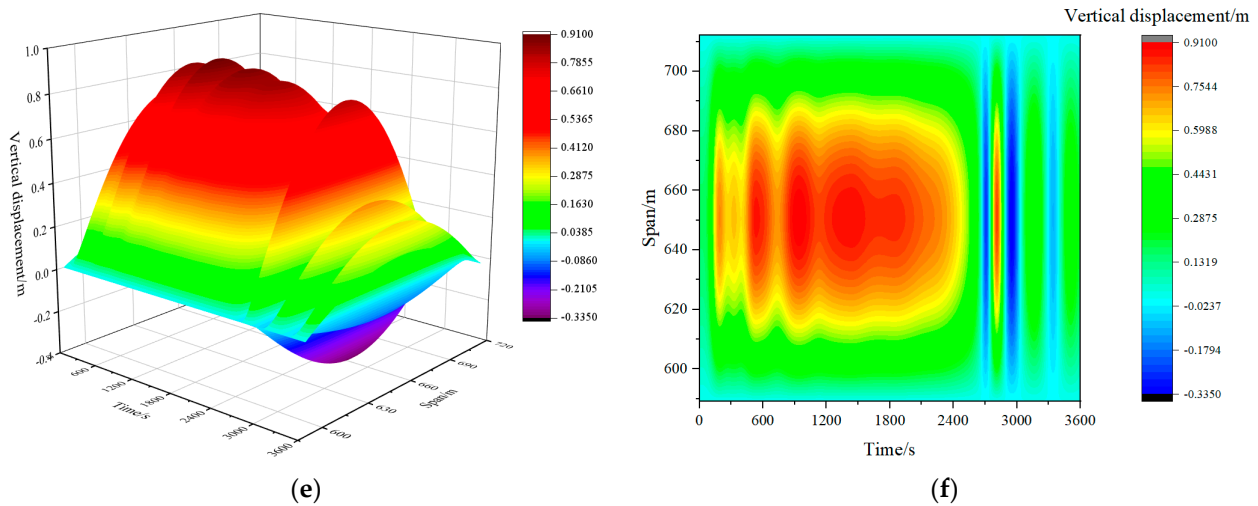


Figure 16. Vertical displacement–time–span 3D relationship of the main cable at design velocity: (a) plot of time–varying displacements of mid–span cables distributed along the span, (b) top view of time–varying displacements of mid–span cables, (c) plot of time–varying displacements of the left–span cords distributed along the span, (d) top view of the time–varying displacement of the left–span cable, (e) plot of time–varying displacements of the right–span cords distributed along the span, (f) top view of time–varying displacements of the right–span cable.

4.3.4. Design Parameter Analysis

In order to analyze the influence of the traveling speed and load of the crane on the vibration, this section takes $\alpha = V_n/V_0$ and $\beta = G_n/G_0$, where V_n is the different speeds and V_0 is the design speed. When $\alpha = 0$, there is a static effect. G_n is the different loads, and G_0 is the design load. When $\beta = 0$, only the crane is acting on the main cables. The top view of the relationship between the design parameters is shown in Figure 17, in which $y(L/2,t)$ indicates the vertical displacement in the span at different moments. y_0 indicates the maximum vertical displacement in the span in the design state. $F(L/2,t)$ indicates the cable force in the span at different moments, and F_0 indicates the maximum cable force in the span in the design state, as shown in Figure 18.

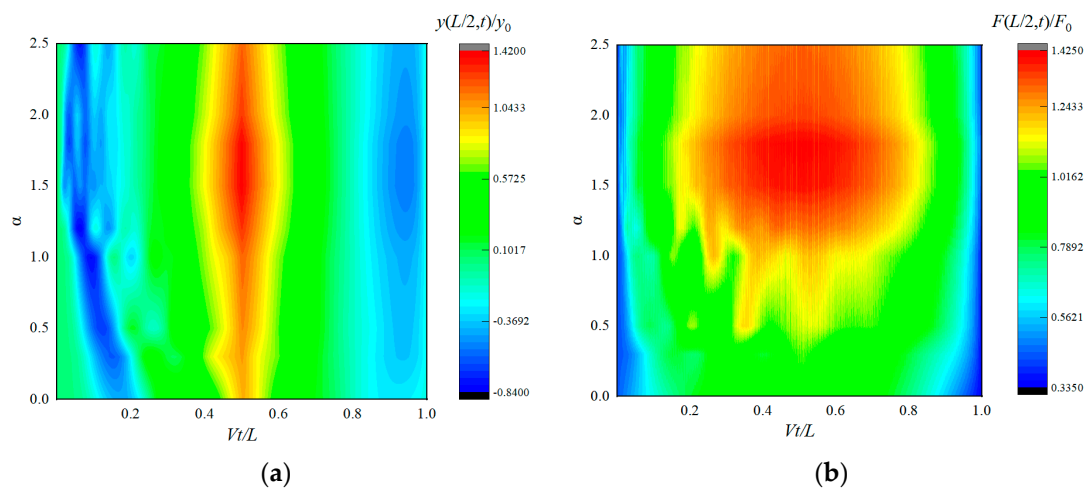


Figure 17. Relative values of mid–span displacement and cable force versus time and velocity parameters: (a) top view of relative values of mid–span displacements, (b) top view of relative values of mid–span cable forces.

From Figures 17 and 18, it can be seen that (1) the traveling speed of the crane is proportional to the vertical displacement in the span, but when the speed exceeds 2 times

the design speed, there is an obvious decreasing trend. The cable force in the span will have an obvious sharp increase when it exceeds the design speed, but there will also be an obvious decreasing trend when it exceeds 2 times the design speed. (2) The load capacity presents an obvious proportionality with the span displacement and cable force, and the vertical displacement will increase sharply when it exceeds 0.7 times the design load capacity. The cable force in the span will increase obviously and reach its peak moment much faster when it exceeds 1.5 times the design load capacity. When the load exceeds 0.7 times the design load, the vertical displacement will increase rapidly.

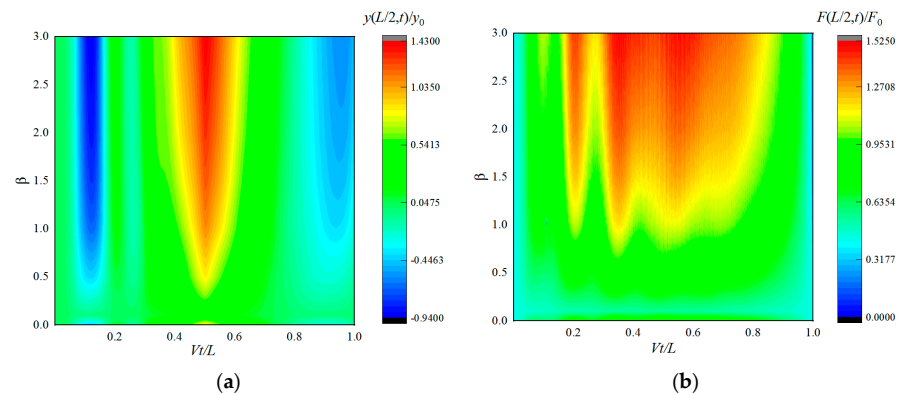


Figure 18. Relative values of mid-span displacement and cable force versus time and load parameters: (a) top view of relative values of mid-span displacements, (b) top view of relative values of mid-span cable forces.

5. Conclusions

To study the nonlinear vibration response of a multi-span continuous cable structure under moving loads considering friction slip, this paper proposes using the direct stiffness method to establish the main cable subsystem model and the moving load model. The coupled vibration control equations are derived through the equilibrium relationship between the moving load and the main cables, and then the dynamics equations are solved based on the Newmark- β direct integration method, so as to obtain the dynamic response of the two. Simulation results were considered for comparison, and the following conclusions were obtained:

- (1) Comparing the calculation results of the self-programmed program, the simulation model results and the dynamic load test values, it can be seen that the calculated results of the first two are in good agreement with the measured values. The errors of the vertical displacement in the span calculated by both of them are 0.86% and -4.40%, but the error reaches -13.90% when the coupled vibration response is not taken into account. This can prove the correctness and rationality of the deduced coupled vibration control equations and programming. It is necessary to consider the coupled vibration of the moving loads and the main cable during the design of the main cable.
- (2) Through the analysis of the impact effect of the cable hoisting system when hoisting weights out of the lifting cable, it can be seen that the instantaneous hoisting of weights out of the coupling vibration generated by the impact effect is very obvious. The impact coefficient of the deflection of the main cable is 2.0. The impact coefficient of the force of the main cable is 2.16. The impact coefficient of the cable tower deflection can be up to 4.0.
- (3) By establishing the vertical displacement-time-span three-dimensional surface diagram of the main cable, it can be seen that during the traveling process of the overhead crane with a load, the vertical downward deflection of the main cable at the point of action is the largest. But the other parts of the cable will show an upward deflection region; the upward deflection region is mainly concentrated in the interval from the

point of action of $0.5L\sim 0.8L$. The closer to the middle of the span, the smaller the upward deflection region. When the crane is traveling away from the main cable of the middle span, the side-span cable is the first one that vibrates downward and reaches the peak value.

- (4) By comparing the relative values of span displacement and cable force with time, crane speed and load parameters, it can be seen that the crane speed is proportional to the vertical displacement in the span. The cable force in the span will show an obvious rapid increase when it exceeds the design speed. When the load exceeds 0.7 times the design load, the vertical displacement will increase rapidly. The cable force in the span will increase rapidly when the load exceeds 1.5 times the design load, and the moment of reaching the peak value will be faster.

Author Contributions: Z.T.: project administration, funding acquisition, conceptualization, formal analysis; B.X.: methodology, formal analysis, investigation, data curation, writing—original draft, writing—review and editing. All authors have read and agreed to the published version of the manuscript.

Funding: This research was funded by the National Natural Science Foundation of China [52078058] and the Hunan Provincial Natural Science Foundation Project of China [2022JJ50323].

Institutional Review Board Statement: Not applicable.

Informed Consent Statement: Not applicable.

Data Availability Statement: All data that support the findings of this study are available from the corresponding author upon reasonable request.

Conflicts of Interest: The authors declare no conflicts of interest.

References

1. Yan, X.L. Cable hoisting technology development and application in bridge engineering. *Int. J. Intell. Inf. Manag. Sci.* **2016**, *5*, 63–68.
2. Huang, Q.; Wu, X.G.; Zhang, Y.F.; Ma, M. Proposed New Analytical Method of Tower Load in Large-Span Arch Bridge Cable Lifting Construction. *Appl. Sci.* **2022**, *12*, 9373. [[CrossRef](#)]
3. Chung, K.S.; Cho, J.Y.; Park, J.I.; Chang, S.P. Three-Dimensional Elastic Catenary Cable Element Considering Sliding Effect. *J. Eng. Mech.* **2011**, *137*, 276–283. [[CrossRef](#)]
4. Kan, Z.Y.; Wu, J.W.; Dong, K.J.; Li, F.; Peng, H.J. A general framework for sliding cable analysis with elastic catenary equation. *Int. J. Solids Struct.* **2021**, *233*, 111290. [[CrossRef](#)]
5. Nizar, B.H.A.; Kan, Z.Y.; Peng, H.J.; Landolf, R.B. On static analysis of tensile structures with sliding cables: The frictional sliding case. *Eng. Comput.* **2021**, *37*, 1429–1442.
6. Nizar, B.H.A.; Omar, A.; Landolf, R.B. A finite element formulation for clustered cables with sliding-induced friction. *Int. J. Space Struct.* **2022**, *37*, 81–93.
7. Yang, M.G.; Chen, S.Z.; Hu, S.T. Nonlinear finite element formulation for sliding cable structures considering frictional, thermal and pulley-dimension effects. *Struct. Eng. Mech.* **2022**, *82*, 205–224.
8. Irvine, H.M.; Caughey, T.K. The Linear Theory of Free Vibrations of a Suspended Cable. *Proc. R. Soc. A* **1974**, *341*, 299–315.
9. Irvine, H.M.; Griffin, J.H. On the dynamic response of a suspended cable. *Earthq. Eng. Struct. Dyn.* **1976**, *4*, 389–402. [[CrossRef](#)]
10. Luongo, A.; Rega, G.; Vestroni, F. Planar non-linear free vibrations of an elastic cable. *Int. J. Non-Linear Mech.* **1984**, *19*, 39–52. [[CrossRef](#)]
11. Hagedorn, P.; Schäfer, B. On non-linear free vibrations of an elastic cable. *Int. J. Non-Linear Mech.* **1980**, *15*, 333–340. [[CrossRef](#)]
12. Al-Noury, S.I.; Ali, S.A. Large-amplitude vibrations of parabolic cables. *J. Sound Vib.* **1985**, *101*, 451–462. [[CrossRef](#)]
13. Shen, G.; Macdonald, J.; Coules, H.E. Nonlinear cable-deck interaction vibrations of cable-stayed bridges. *J. Sound Vib.* **2023**, *544*, 117428. [[CrossRef](#)]
14. Benedettini, F.; Rega, G. Non-linear dynamics of an elastic cable under planar excitation. *Int. J. Non-Linear Mech.* **1987**, *22*, 497–509. [[CrossRef](#)]
15. Chen, C.C.; Wu, J.S. The dynamic analysis of a suspended cable due to a moving load. *Int. J. Numer. Methods Eng.* **1989**, *28*, 2361–2381.
16. Ledezma-Ramírez, D.F.; Tapia-González, P.E.; Brennan, M.J.; Paupitz Gonçalves, P.J. An experimental investigation into the shock response of a compact wire cable isolator in its axial direction. *Eng. Struct.* **2022**, *262*, 114317. [[CrossRef](#)]
17. Stricklin, J.A.; Haisler, W.E. Formulations and solution procedures for nonlinear structural analysis. *Comput. Struct.* **1977**, *7*, 125–136. [[CrossRef](#)]

18. Filho, F.V.; Coutinho, A.L.G.A.; Landau, L.; Lima, E.C.P.; Ebecken, N.F.F. Nonlinear dynamic analysis using the pseudo-force method and the Lanczos-algorithm. *Comput. Struct.* **1988**, *30*, 979–983. [[CrossRef](#)]
19. Bathe, K.J.; Gracewski, S. On non-linear dynamic analysis using substructuring and mode superposition. *Comput. Struct.* **1981**, *13*, 699–707. [[CrossRef](#)]
20. Bijan Mohraz, B.; Fawzi, E.E.; Chang, C.J. An incremental mode-superposition for non-linear dynamic analysis. *Earthq. Eng. Struct. Dyn.* **1991**, *20*, 471–481. [[CrossRef](#)]
21. Kovacic, I.; Brennan, M.J. *The Duffing Equation: Nonlinear Oscillators and Their Behaviour*; Wiley: Hoboken, NJ, USA, 2011; pp. 44–45.
22. Luo, H.; Zhang, X.; Cui, K.; Chen, K. A multi-scale model-order reduction strategy for vibration analysis of coupled structures with local inhomogeneities. *Comput. Struct.* **2024**, *290*, 107191. [[CrossRef](#)]
23. Han, F.; Dan, D.H.; Cheng, W. Extension of dynamic stiffness method to complicated damped structures. *Comput. Struct.* **2018**, *208*, 143–150. [[CrossRef](#)]
24. Han, F.; Dan, D.H.; Wei, C.; Zang, J.B. An improved Wittrick-Williams algorithm for beam-type structures. *Compos. Struct.* **2018**, *204*, 560–566. [[CrossRef](#)]
25. Dan, D.H.; Han, F.; Cheng, W.; Xu, B. Unified modal analysis of complex cable systems via extended dynamic stiffness method and enhanced computation. *Struct. Control Health Monit.* **2019**, *26*, e2435. [[CrossRef](#)]
26. Han, F.; Dan, D.H. Free vibration of the complex cable system-An exact method using symbolic computation. *Mech. Syst. Signal Process.* **2020**, *139*, 106636.
27. Arturo, G.; Enrique, C.; Miguel, C. Verifying the suitability of uncoupled numerical methods for solving vehicle-bridge interaction problems. *Struct. Infrastruct. Eng. Maint. Manag. Life-Cycle Des. Perform.* **2022**, *19*, 1407–1424.
28. Thai, H.T.; Kim, S.E. Nonlinear static and dynamic analysis of cable structures. *Finite Elem. Anal. Des.* **2011**, *47*, 237–246. [[CrossRef](#)]
29. Cong, Y.Y.; Kang, H.J.; Guo, T.D.; Su, X.Y. One-to-one internal resonance of a cable-beam structure subjected to a concentrated load. *J. Sound Vib.* **2022**, *529*, 116915. [[CrossRef](#)]

Disclaimer/Publisher’s Note: The statements, opinions and data contained in all publications are solely those of the individual author(s) and contributor(s) and not of MDPI and/or the editor(s). MDPI and/or the editor(s) disclaim responsibility for any injury to people or property resulting from any ideas, methods, instructions or products referred to in the content.